2022

Infrared-Thermography And Numerical Investigation Of Conjugate Heat Transfer In Roots Blower

Brijeshkumar Patel

Sham Rane

Ahmed Kovacevic

Infrared-Thermography and numerical investigation of conjugate heat transfer in Roots blower

Brijeshkumar PATEL[1]*, Sham RANE[2], Ahmed KOVACEVIC[3]

[1,2,3] City, University of London, London, UK, EC1V0HB

[1]brijeshkumar.patel@city.ac.uk
[2]sham.rane@city.ac.uk
[3]a.kovacevic@city.ac.uk

* Corresponding Author

ABSTRACT

In Positive displacement machines, operating temperature of the gas is different than the rotor and casing temperatures, causing heat to flow from gas to rotors and casing and vice versa. Thermal expansion of the machine components which occurs at high speed, changes operating clearances between rotors and the casing. This leads to deterioration of efficiency and reliability of the machine. The present research work focuses on both, the experimental study of heat transfer at the rotor surface during the operation of the machine and on development and validation of CFD models. The heat transfer phenomenon between solid and fluid is treated in the numerical model as conjugate heat transfer (CHT).

An experimental study on an optically accessible roots blower is performed using a high-speed infrared thermography system. Required optical access on the machine is constructed from sapphire glass. National Instrument-based data acquisition system is designed to achieve phase-lock synchronization of the camera exposure with the rotation angle of the lobe. This system is also extended to measure and control machine operating parameters such as pressure, temperature, flow, power, and speed. A CFD model of the experimental Roots Blower was evaluated with fluid flow and conjugate heat transfer. Additional complexity of the model involved deforming rotor grids and in-house tool SCORG was used for this purpose. Results of steady state lobe surface temperature and housing external temperature have been verified in the numerical model at various operating conditions. This CHT model will be used in future to evaluate design modification and conceptualize methods for reduction in leakage losses and ensure reliable operation of the machine.

Keywords: Positive displacement machines, Infrared thermography, Conjugate heat transfer, Computational fluid dynamics

1. INTRODUCTION

Rotary machines are present in the majority of energy generation and conversion systems. Today's compressed air sector utilizes almost 20% of a world generated power, which is why these machines contribute highly in carbon emission (Vittorini, Bianchi, & Cipollone, 2015). So, this study focuses explicitly on oil-free rotary machines. As depicted in Figure 1, all rotary machines have a clearance gap to allow motion between stator and rotor, and these clearance gaps are one of the significant contributors to efficiency loss. Nowadays, it is possible to maintain optimal clearance gap in rotary machines, but it introduces question on the reliability of machines as clearance gap size varies in running condition.

Most experimental research in positive displacement machines was carried out to measure the temperature and heat transfer of outer part of the machine (Zhang & Wu, 2021). But it is extremely important to study temperature variation of inner part, most importantly rotary part of the machine. Far fewer experimental studies have been performed at engine running conditions due to the complexities of testing at high speed (Rane, Stosic, & Dhunput, 2014). Therefore, present study focuses on the measurement of lobe surface temperature and Outer body

temperature in the running condition of the machine. High speed infrared camera is selected from Infratec which is able to capture the lobe surface temperature during the running condition of the machine.
The computational model for positive displacement machines such as twin-screw compressors has been described in Kovačević (2005, 2007) and is widely applicable, such as for the presented Roots blower model. Rane (2017a, 2017b, 2021a) and Kovačević (2017) have presented the development and application of different types of deforming grid topologies that can be used for modelling of twin-screw machines. Applications to dry air and oil injected compressors and ORC expanders have been investigated. A bi-directional coupling of fluid flow and structural solvers was reported by Rane *et al*. (2021b). The application was for a dry air twin-screw compressor. Conjugate heat transfer (CHT) model was used to produce boundary conditions required for the structural solver that evaluated the local leakage gap variation, in turn this was supplied to the CFD – CHT model to update the flow field. Even for the Roots blower CFD model, the deforming rotor grid is a critical element of the setup as it directly controls the interlobe and radial gap sizes. Additionally, the rotor profiles have a stepped tip design which can result into local flow features of importance. Singh *et al*. (2019) have presented a detailed analysis of this machine while operating at low-speed conditions. PIV data of the flow in working chamber was used to evaluate the numerical model. In their study, the rotor grids that were used consisted of fixed nodes on the profile and rotating plus sliding nodes on the housing and the non-conformal interface between the two rotors, called as rotor-to-casing topology (Rane, 2017b). Eettisseri *et al.* (2021) have analysed heat transfer mapping inside a reciprocating hermetic compressor by considering the rotation of crankshaft and associated motion of connecting rod and piston in a CHT model with Immersed Solid Method in the ANSYS CFX solver. Dincer *et al.* (2017) have presented a non-isothermal CFD analyses of a hermetic reciprocating compressor by means of evaluating the CHT in steady and transient models. In centrifugal compressors, CHT studies are a common design analysis practice, and several studies are available in literature (Gu *et al.*, 2015, Moosania & Zheng, 2016, Roclawski *et al.*, 2016, Stahl *et al.*, 2019). However, in case of positive displacement machines such as twin-screw compressors or Roots blower, detailed CHT analysis are not yet available. In the numerical part of the present study, the goal was to develop a full CHT model of the Roots blower machine and use the Infrared-Thermography experimental data for the validation of the modelling procedures. Such a validated CFD – CHT model could then be used to investigate in detail, the impact of heat transfer on leakage flows and thereby improve the design and performance of the machine.

2. INFRARED-THERMOGRAPHY EXPERIMENTAL METHOD

Infrared-Thermography experimental method consist of three major set of elements, 1). Optical roots blower 2). Roots blower test rig and 3). High speed infrared thermography setup.

2.1. Optical roots blower

In this study, Roots blower URAI-22 from Howden is used. Optical access is required on the Roots blower to visualize the temperature field in the clearances. To get optical access of radial leakage path some portion (Area bounded by the yellow line in Figure 1) of the Roots blower is replaced by optical material. For the current application, optical material should be able to withstand high temperature and pressure up to 300 °C and 7 barg respectively. Besides, specifically for infrared thermography technique, the optical element should be transparent for Infrared spectrum of light.

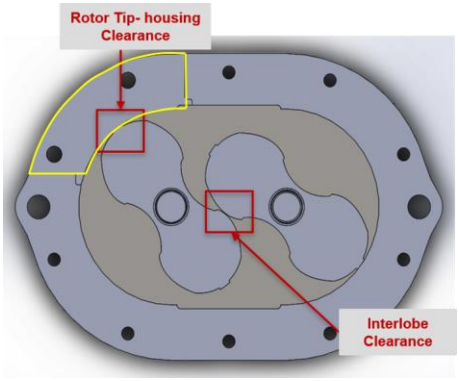

Figure 1: Clearances in Roots blower

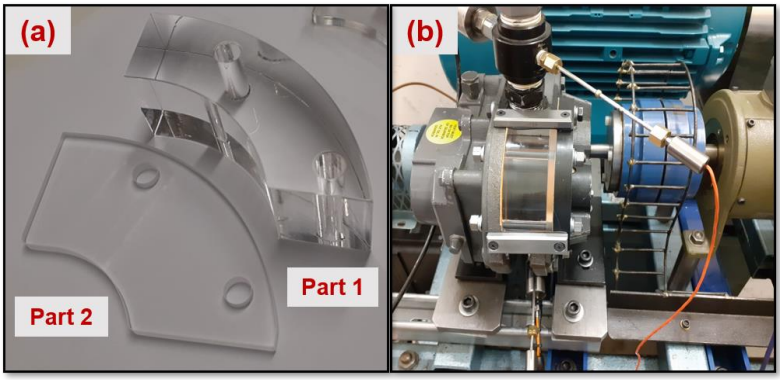

Figure 2: (a) Optical element from Sapphire Glass, (b) Radial optical access of Roots blower

For optical access, Sapphire glass is the best suitable material for our application. Figure 2 (a) shows a complex shape of the optical Glass manufactured from the Sapphire. As shown in Figure 2 (b), Optical access from radial direction of the Roots blower is provided to visualize a surface of the rotor tip in running condition. A thin gasket is used between metal and Glass surface to avoid any direct contact to reduce risk of cracking in the Glass at higher working temperature. Glass is kept tight using an external metal plate to eliminate leakage through glass and metal mating surfaces.

2.2. Roots blower test rig

The layout of the Roots blower test rig is depicted in Figure 3. Roots blower is connected with variable speed electric motor through pulley transmission system to run at various operating condition, and Roots blower can run up to 2700 RPM based on current pulley ratio. To monitor and control the operating parameter of the machine, pressure and temperature sensors are installed at suction (P1, T1), discharge (P2, T2) and Orifice (ΔP, T3). Shaft encoder and torque meter are used to measure the speed and power of roots blower. The flow of the machine measures using Orifice. The ball valve is installed in the discharge line of the machine require discharge pressure. By partially closing the valve, we can increase the discharge pressure of the machine. All sensors are connected with National instrument-based data acquisition system, and real-time data are recorded using LabView based programming. This experiment only uses ambient air as a working fluid, for that Nitrogen and anisole supply is bypassed here.

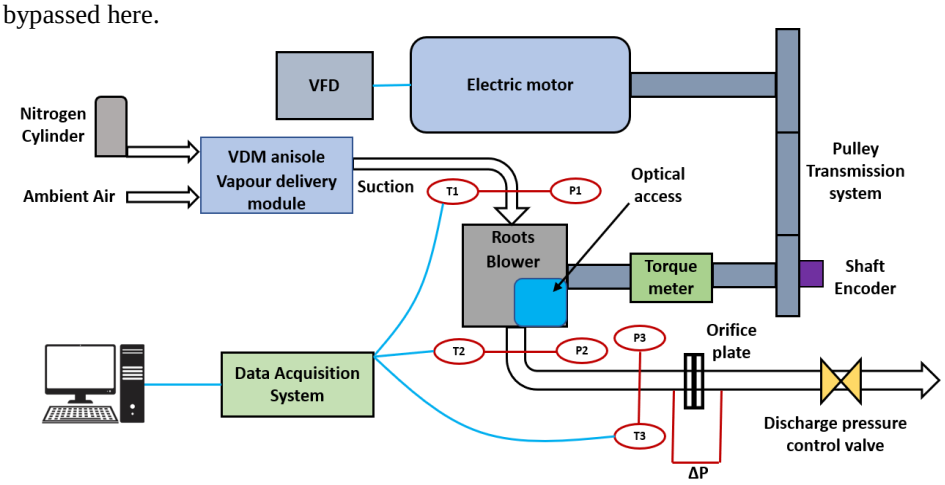

Figure 3: Layout of the Roots blower test rig (Patel, Kovacevic, Charogiannis, Alam, & Schütte, 2021)

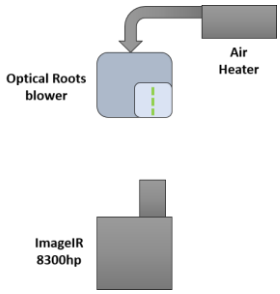

Figure 4: High-speed infrared thermography

2.3. High speed infrared thermography test setup

IR thermography has been widely used for surface temperature measurement and it provides an effective approach for non-intrusive and spatial-temporal measurement of temperature.

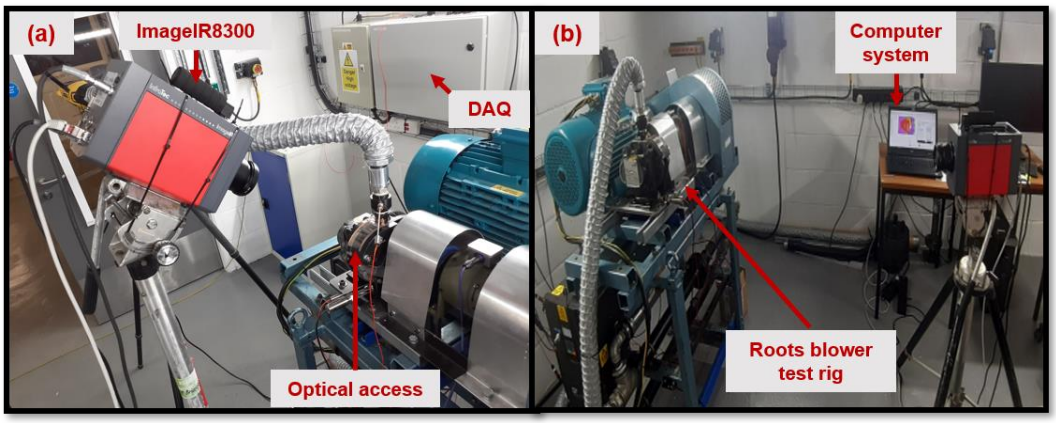

Figure 5: (a) IR camera focused on the lobe surface, (b) IR camera focused on the entire Roots blower

Usually, this technique is applicable for surface temperature measurement. In order to determine temperatures accurately with IR Thermography, careful attention toward a proper choice of windows, elimination of specular reflections from channel walls, and estimation of local emissivity changes are required. The principle of infrared thermography is based on the physical phenomenon that any body of a temperature above absolute zero (-273.15 °C) emits electromagnetic radiation. There is clear correlation between the surface of a body and the intensity and spectral composition of its emitted radiation (Speakman, 2019). By determining its radiation intensity, the temperature of an object can thereby be determined in a non-contact way. ImageIR 8300hp camera has been chosen, it has spectral range of 2 to 5.7 µm, and temperature range of -40 to 1500 °C with full frame rate of 355Hz. The layout of the setup and actual setup is shown in Figure 5. To measure the lobe surface temperature during the running condition of the machine Phase lock is achieved by triggering the camera using the shaft encoder signal and LabView programming.

3. CFD AND CONJUGATE HEAT TRANSFER MODEL

The goal of the numerical analysis was to develop a detailed conjugate heat transfer model of the Roots blower machine and use the Infrared-Thermography experimental data for the validation of the modelling procedures. Figure 6 shows the main components of the CFD – CHT model. Figure 6a are the fluid parts that consist of the deforming rotor domains, suction and discharge ports and extended inlet and outlet pipes for applying boundary conditions. Figure 6b shows the CHT solid parts that consist of the rotor housing, gear-box housing, the main and the gate rotor, sapphire glass and the fixing plate. The entire model was complex with 12 domains, 9 fluid-fluid interfaces, 4 solid-solid interfaces and 7 fluid-solid interfaces. Validation of the CFD – CHT model is required to satisfy the following quantitative data: **a.** Cycle averaged gas flow rate and the indicated power needs to be validated with the measured blower performance data, **b.** Cycle averaged gas temperature at the discharge needs to be within small deviation compared with the measured gas temperature and **c.** Quantitative surface temperature data typically obtained on the rotor lobes and the housing's external surfaces needs to be within the range of prediction obtained from thermograms.

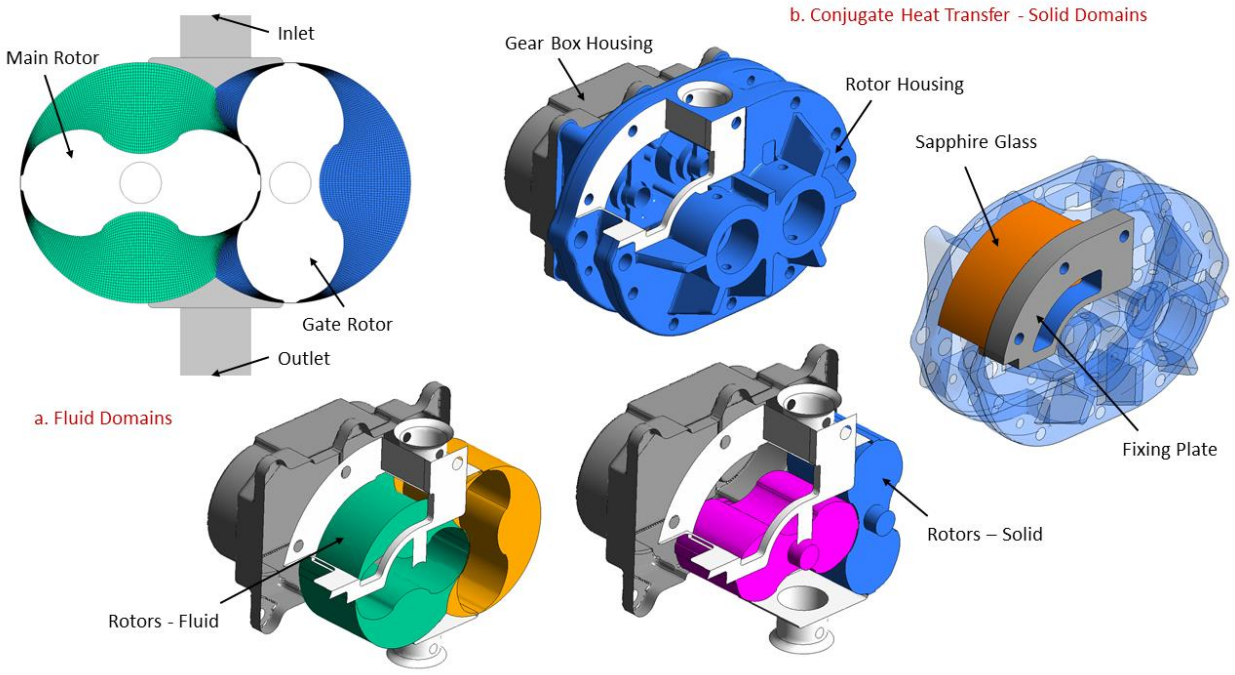

Figure 6: Components of the numerical model, (a) CFD – Fluid domains, (b) CHT – Solid domains

3.1. Grid Generation Consideration

SCORG grid generator (Kovačević and Rane, 2017) was used for the deforming rotor grid generation and ANSYS meshing tools were used for the stationary fluid domains as well as all the solid domains. A hexahedral cell structure as shown in Figure 6a is preferred in the deforming rotor domain. Other components have a combination of hexahedral and tetrahedral cell structure in order to conform with the geometry of the ports and the blower housing.

During the study it was found that the rotor-to-casing type of deforming rotor grid have a single housing boundary surface for each rotor domain. This surface forms a fluid-fluid non-conformal interface between the rotors and also interface simultaneously with the suction and discharge ports. The numerical solver ANSYS CFX limits the boundary surfaces to be used in one type of interface, either fluid-fluid or fluid-solid. This limited the development of a fluid-solid interface between the deforming fluid rotor grid and the housing. Using SCORG, the topology of the rotor grid was then changed to a Casing-to-Rotor non-conformal type. This deforming rotor grid topology allowed the housing surface to be split into sub-areas that could be individually used in the fluid-fluid and fluid-solid interfaces. The total node count in the deforming rotor domain was 576,600, in the stationary fluid domain was 889,405, in the housing, fixing plat and the solid rotors was 289,732 and in the sapphire glass domain was 11770. The whole CFD – CHT model size was thus close to 1767507 nodes.

3.2. Numerical Solver

ANSYS CFX which is a well validated CFD solver in the application of positive displacement machines was used in the current study. Singh *et al*. (2020) have used the same solver in their PIV based investigation. Table 1 provides the specification of material properties used in the model setup. The sapphire glass used to provide optical access for Infrared-Thermography has a lower thermal conductivity and higher specific heat capacity in comparison to the main housing and rotor material which was steel.

Table 1: Material specification for the components of the model

Component	**Material**	**Density**	**Dynamic Viscosity**	**Thermal Conductivity**	**Specific Heat**
		[kg m^{-3}]	[kg m^{-1} sec^{-1}]	[W m^{-1} K^{-1}]	[J kg^{-1} K^{-1}]
Gas	Air	Ideal Gas Law	1.831E-05	0.0261	1004.4
Rotors **Gear Box Housing** **Rotor Housing**	Steel	7854.0	-	60.50	434.0
Sapphire Glass	Glass	3970.0	-	27.21	763.0
Fixing Plate	Steel	7854.0	-	60.50	434.0

Table 2 provides the specification of the important parameters of the numerical solver. Special attention in a CHT numerical model is required for the parameter CHT Time Scaling factors. This parameter acts like an accelerator for heat conduction through the solid components and helps in saving computational time which could be too high otherwise. This is due to the large time scale disparity between fluid flow and solid heat transfer. In the present study, at the rotor speed of 2000 rpm as an example, the fluid flow time steps size was $8.3333e^{-05}$ sec. Whereas Infrared-Thermography test data has been collected at a time span of the order of 10 -15 minutes. Hence a CHT time scale factor serves to reach this test data time span without the need to calculate the flow field over the full time duration. A sensitivity analysis was carried out by varying the CHT time scale in the range 1- 100000 and the results are presented in the next section.

Table 2: Specification of the numerical setup in the ANSYS CFX solver

Rotor mesh deformation	User defined nodal displacement	Advection scheme	High Resolution
Mesh in ports	Tetrahedral with boundary layer refinements (ANSYS Mesh)	Transient scheme	Second order Backward Euler
Mesh in solid parts	Tetrahedral with curvature refinement (ANSYS Mesh)	CHT Time Scaling	1 - 100000
Turbulence model	SST – k Omega (Standard Wall Functions)	Transient inner loop coefficients	Up to 20 iterations per time step
Inlet/Supercharge boundary condition	Opening (Specified total pressure and temperature)	Convergence criteria	r.m.s residual level $1e^{-03}$
Outlet boundary condition	Opening (Static pressure, backflow acts as total pressure and temperature)	Relaxation parameters	Solver relaxation fluids (0.4)

To achieve the objective ‘a’ of model validation while keeping the computational size in limits, an initial study for gap size calibration was conducted with the CFD model that did not include CHT and the solid parts. In this setup

the deforming rotor grids were generated with 100 µm gap size in the radial and interlobe leakage gaps. The axial gaps on both ends of the rotor were added as stationary domains and the axial gaps size was calibrated to achieve the measured flow and indicated power. The results have been presented in the next section. These calibrated gap sizes for each operating condition were then used to setup the CHT model with solid domains and used for the evaluation of objectives 'b' and 'c' of model validation.

4. RESULTS AND DISCUSSION

The Roots blower was operated at set of rotor speed and pressure ratio such that the discharge gas temperature varied in the range from 50°C to 150°C. At each operating condition, when stable temperatures were reached, the thermograms were recorded. Performance of the blower and a sample thermogram is discussed here. Results from the numerical analysis and a sample comparison with the measured thermogram is also discussed.

4.1. Experimental results

Lobe surface temperature is measured at various machine operating conditions. As shown in Table 3, machine was operated at various speed ranging from 1000 RPM to 2000 RPM and pressure ratio ranging from 1.2 to 1.6. Machine discharge temperature (T2) was allowed to stabilize at each operating condition and series of 500 thermal images are captured.

Table 3: Measurements at various machine running conditions

Pressure Ratio (P2/P1)	Blower speed	Suction temperature, T1	Discharge temperature, T2	Vol Air flow	Mass flow rate	Power
	[rpm]	[°C]	[°C]	[m^3 min^{-1}]	[kg sec^{-1}]	[kW]
1.212	999.98	29.66	52.46	0.1686	0.0033	0.230
1.203	1499.26	29.19	59.06	0.3182	0.0063	0.323
1.202	1999.26	30.03	57.72	0.4698	0.0092	0.437
1.406	1998.37	30.92	82.31	0.3970	0.0078	0.760
1.599	2000.84	33.80	139.05	0.3627	0.0070	1.056

Thermograms obtained at 2000 RPM and 1.6 PR is presented in Figure 7. It shows the lobe surface temperature at mentioned condition during stabilized discharge temperature of the machine. From the data it is observed that temperature difference across the tip is around 1 °C and across the lobe is around 2.5 °C at 2000 RPM and 1.6 PR. It is also found that temperature difference remains nearly the same at each pressure ratio but overall surface temperature is different. This measurement data is used to validate CFD – CHT numerical model.

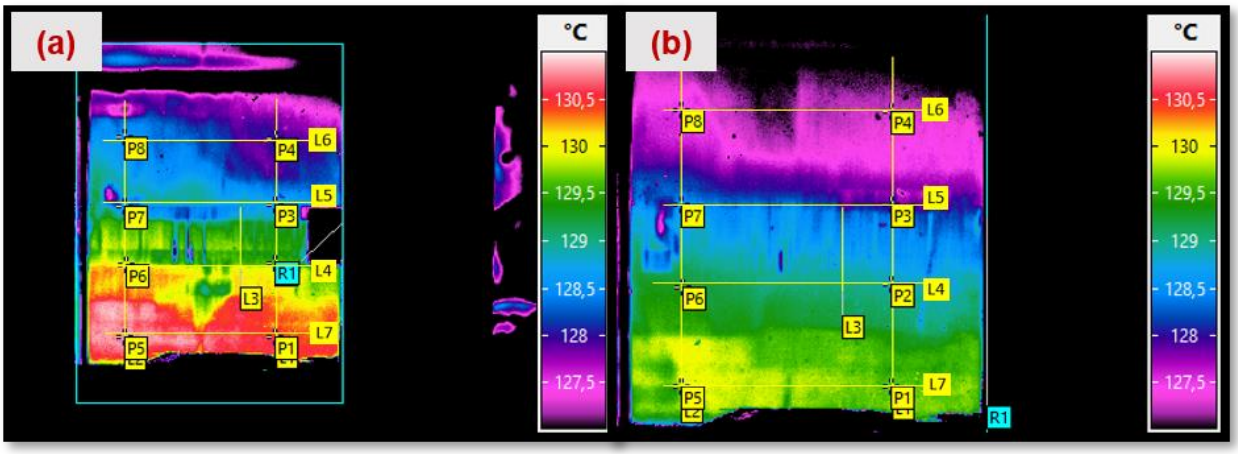

Figure 7: (a) Thermogram of Tip 1, (b) Thermogram of Tip 2 of lobe at 2000RPM and 1.6 PR

4.2. CFD Model Leakage Gap Calibration

Figure 1 shows a cut section across the Roots blower and the leakage gaps formed between the rotors and the housing. There are tip radial gaps between the two rotors and the housing with a design specification of 100 µm and interlobe clearance gap is between the two rotors with a design specification of 100 µm. On axial end of the rotor, there are axial clearance gaps with a design specification of 150 µm.

Objective 'a' of the CFD – CHT model is to achieve a cyclically averaged gas flow rate and the indicated power close to the measured blower performance data provided in Table 3 at various operating conditions. Before the full CHT model was evaluated, an initial study for gap size calibration was conducted with the CFD model that did not include the solid parts. In this initial gap calibration setup, the deforming rotor grids were generated with 100 µm gap size in the radial and interlobe leakage gaps. This allowed the use of a common deforming rotor mesh at all operating conditions of Table 3. Whereas the axial gaps on both ends of the rotor were added as stationary domains and the gap size was calibrated (iteratively varied) to achieve the measured flow and indicated power.

Table 4: Calibration of the leakage gap size

Pressure Ratio	Blower Speed	Mass flow rate	Deviation	Power	Deviation	Calibrated Gap Size	Mechanical η
	[rpm]	[kg sec^{-1}]	[%]	[kW]	[%]	[um]	[%]
1.212	999.98	0.00312	5.33	0.1683	1.66	100	72
1.203	1499.26	0.00616	2.18	0.2460	2.09	150	74.5
1.202	1999.26	0.00988	7.39	0.3336	2.47	170	74.5
1.406	1998.37	0.00831	6.52	0.6576	1.80	110	85
1.599	2000.84	0.00731	4.40	0.9599	1.00	70	90

Table 4 provides the gap calibration data from the CFD model. The maximum deviation in gas flow rate is below 8% and that in the indicated power is below 2.5%. Indicated power in the measured data was obtained by assuming a mechanical efficiency of the order 72 – 90 %. At lower speed of 1000 rpm and lower pressure ratio of 1.2, the axial gap size was required to be reduced from design specification of 150 µm to 100 µm. As rotor speed was increased for this pressure ratio, the gap size requirement was 150 µm and 170 µm at 1500 rpm and 2000 rpm respectively. However, at 2000 rpm, when the pressure ratio was increased to 1.4 and 1.6, the axial gap sizes were further required to be lowered to 110 µm and 70 µm respectively, to account for a relatively higher leakage. The blower rotors are driven by a synchronizing gear box that is grease lubricated. It was observed that with increasing speed, the mechanical efficiency did not vary much and was about 72 – 75%. But when the pressure ratio increased, resulting into higher discharge temperature, the mechanical efficiency improved to 85% and 90 % at pressure ratio 1.4 and 1.6 respectively. This could be due to lower grease viscosity as the temperature increased. Table 4 calibrated gap sizes for each operating condition were then used to setup the full CHT model described in Figure 6 with the solid domains.

4.3. Internal gas temperature distribution

During the cyclic operation of the Roots blower, the gas temperature is highly fluctuating. At an operating speed of 2000 rpm and pressure ratio 1.6, the local variation of gas temperature has been presented in Figure 8 at few rotor positions. These results are from the model setup for calibration of the leakage gaps.

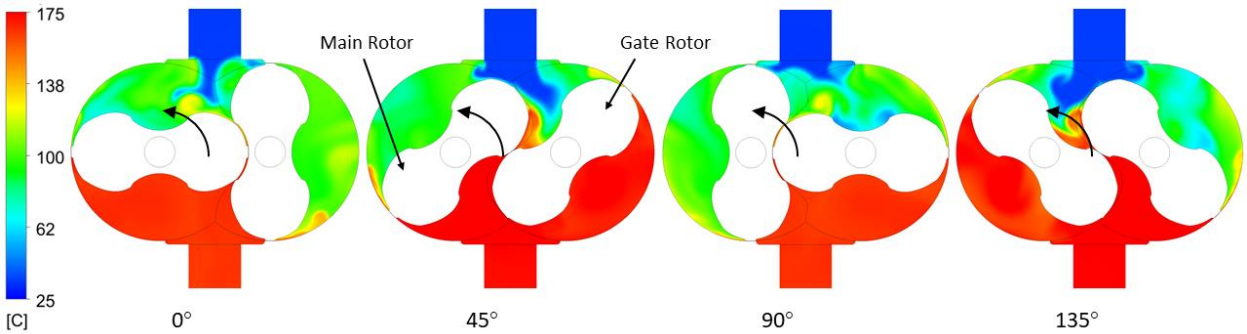

Figure 8: Gas temperature at various rotor positions for 2000 rpm, 1.6 pressure ratio operating condition

Due to leakage and recompression, the exit gas temperature reaches close to 175°C. The measured data at this operating condition has discharge temperature of 139°C. The difference in temperature from the CFD model is due to absence of solid components and associated conjugate heat transfer effects. Due to adiabatic boundary conditions on the rotor and the housing, there is over prediction of the gas temperature rise. At the 0° rotor position, low temperature gas at 25°C is seen to flow and fix in the main rotor chamber. At the interlobe gap and both the tip gaps, higher temperature gas is seen to leak into the succeeding chambers. Further at 45° rotor position, the suction gas switches from main rotor chamber and is seen to fill the gate rotor chamber. High temperature gas leakage in the interlobe is stronger at this rotor position. At 90° and 135° rotor positions the temperature field is similar to that at 0° and 45° positions respectively, except for the filling in main rotor chamber. Similar observations have been made at the other operating conditions of the Roots blower and the CFD model.

4.4. Conjugate Heat Transfer Analysis

Results from the full CHT model described in Figure 6 with the solid domains, at an operating condition of 2000 rpm and pressure ratio 1.6 have been discussed here. As highlighted in the numerical solver specification, the CHT time Scale factor is an important parameter of the CHT model. For the objectives 'b' and 'c' of the validation the CHT time scale factor sensitivity was analysed by varying it in a range from 1 to 100000. Figure 9 presents the temperature distribution in the mid-plane of the bower and represents fluid as well as solid components. A local thermal scale is shown to highlight the impact on exit gas temperature and the distribution within the blower components.

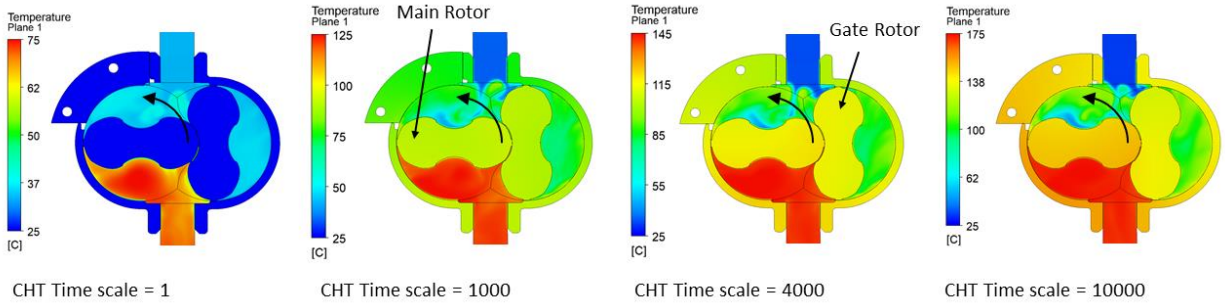

Figure 9: Comparison of temperature distribution in the fluid and solid parts with varying CHT Time Scales

At 2000 rpm rotor speed, the fluid flow time step size is $8.33333e^{-05}$ sec. When the CHT Time scale is 1, the same time step size is applied to heat conduction in the solid components. When the CHT Time scale factor is increased to 1000, 4000 and 10000, the heat conduction in the solid components gets accelerated and the corresponding CHT time steps size are $8.33333e^{-02}$ sec, $3.33333e^{-03}$ sec and $8.33333e^{-01}$ sec respectively. Figure 9 shows that with a CHT Time scale 1, the temperature distribution in the gas has reached cyclic operating levels with a discharge gas temperature close to 75°C. However, the solid components are still close to the cold initial condition of 25°C. With an increment of CHT Time scale to 1000, the discharge gas temperature increases to 125°C and the solid component temperature increases from 25°C to around 80°C in the rotors and 70°C in the housing. At CHT Time scale of 4000, discharge gas temperature is 140°C, rotor temperature 115°C and housing around 100°C. Sapphire glass being of a lower thermal conductivity is at a relatively lower temperature of 85°C. Similar pattern is seen with CHT Time scale 10000, with discharge gas temperature 175°C and rotor close to 140°C. It is also noticed that very high CHT Time scale results into unequal temperatures in the two rotors at this position which is incorrect. In addition, a comparison with measured discharge gas temperature in Table 3 shows that the discharge gas temperature is 139.05°C. Thus, CHT Time scale of 4000 was found to be appropriate for this operating condition to validate the discharge gas temperature objective 'b', but still objective 'c' i.e., rotor surface temperature remains underestimated.

For this purpose, a set of varying initial solid component temperature were studied from 25°C to 125°C. The results from Infrared-Thermography measurement are shown in Figure 10a and the CFD – CHT model results at varying initial temperatures are shown in Figure 10b to Figure 10e. Figure 10b is the rotor surface temperature distribution at 25°C initial condition and a CHT Time scale of 4000, equivalent to 40 min operation. These conditions match the discharge gas temperature at 140°C, but underestimate the rotor surface temperature by about 12°C, in the range 114.5 – 117.5°C. The span of 3°C matches well with the thermogram. Figure 10c is the rotor surface temperature result at 25°C initial condition and a CHT Time scale of 10000, equivalent to 100 min operation. These conditions exceed the discharge gas temperature at 165°C, and overestimate the rotor surface temperature by about 10°C, in the

range 138.5 – 140.5℃. The span of 3℃ matches with the thermogram. Similarly, Figure 10d is the rotor surface temperature result at 80℃ initial condition and a CHT Time scale of 4000, equivalent to 20 min operation. These conditions match the discharge gas temperature at 140℃, and underestimate the rotor surface temperature by about 12℃, in the range 114 – 117℃. By setting a higher initial temperature of 80℃ in the solid components, result equivalent to Figure 10b was obtained, but with half the calculation duration and equivalent operating time (20 min).

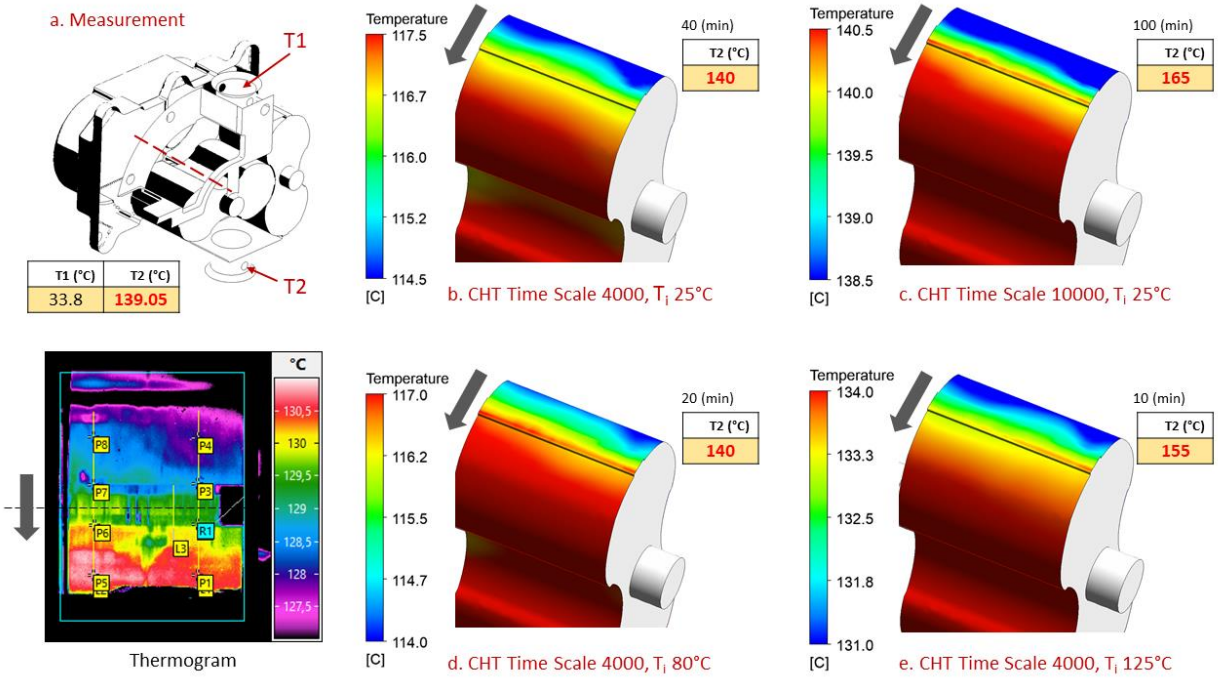

Figure 10: Comparison of rotor lobe surface temperature, (a) Measurement, (b) CHT Time Scale 4000, T_i 25°C, (c) CHT Time Scale 10000, T_i 25°C, (d) CHT Time Scale 4000, T_i 80°C, (e) CHT Time Scale 4000, T_i 125°C

Figure 10e is the rotor surface temperature result at 125℃ initial condition and a CHT Time scale of 4000, equivalent to 10 min operation. These conditions exceed the discharge gas temperature at 155℃, but the rotor surface temperature matches the thermogram closely in the range 131 – 134℃ and a span of 3℃. The overestimate of discharge gas temperature by 15℃ could be attributed to the adiabatic boundary conditions being applied on the housing exterior surfaces.

5. CONCLUSIONS

In summary, this study focuses on the development of the numerical model for CHT and validation of model using experimental data. High speed infrared thermography test setup is developed to measure lobe surface temperature during running conditions of the machine. Thermograms are successfully captured at three various pressure ratios 1.2, 1.4 and 1.6, and speed ranging from 1000 RPM to 2000 RPM. This measurement provides quantitative data for the validation of the developed numerical model.

For the numerical analysis, a full CFD – CHT model of the Roots blower was developed. The analysis and validation objectives were achieved by first evaluating a gap calibration model, followed by CHT analysis.

- The gap analysis provided axial clearance sizes that were able to validate the flow within 8% and indicated power within 2.5% deviation from the measured performance data.
- The full CFD – CHT model was studied in detail, and it was found that the solver parameter of CHT Time scale and the initial temperature of the solid components are critical for the results.
- With an initial temperature in the solid domains at 125℃, and a CHT Time scale of 4000, equivalent to 10 min blower operation, the discharge gas temperature was achieved at 155℃. While the rotor surface temperature was achieved in the range 131 – 134℃ and a span of 3℃, which was close to the thermogram data. An overestimate of discharge gas temperature by 15℃ could be attributed to the adiabatic boundary conditions being applied on the housing exterior surfaces.

In future studies, other operating conditions, and tests with non-adiabatic exterior boundary conditions on the blower exterior surfaces will be evaluated. The CHT model will be used in future to evaluate design modification and conceptualize methods for reduction in leakage losses and ensure reliable operation of the machine.

NOMENCLATURE

P	Pressure	(barg)
T	Temperature	(°C)
T_i	Initial temperature of solid components	(°C)

REFERENCES

Dincer, M., Sarioglu, K. & Gunes, H. (2017). A conjugate heat transfer analysis of a hermetic reciprocating compressor. 10th Int Conf on Compressors and their Systems, London. IOP Conf. Ser.: Mater. Sci. Eng. 232 012010

Eettisseri, R., Real, M., & Oliveira, S. (2021). Analysis Of Dynamic Heat Transfer Coefficient In a Reciprocating Compressor By Immersed Solid Method in CFD. Int Compressor Engineering Conference. Purdue. Paper 2653.

Gu L., Zemp A. & Abhari R. (2015). Numerical study of the heat transfer effect on a centrifugal compressor performance. Proc IMechE Par t C: J Mechanical Engineering Science 2015, Vo l. 229(12) 2207–2220.

Kovačević, A. (2005). Boundary Adaptation in Grid Generation for CFD Analysis of Screw Compressors, *Int. Num. Eng*., 64(3), 401-426.

Kovačević, A., Stošić, N. & Smith, I. K. (2007). *Screw compressors - Three dimensional computational fluid dynamics and solid fluid interaction*, ISBN 3-540-36302-5, Springer-Verlag Berlin Heidelberg New York.

Kovačević, A. & Rane, S. (2017). Algebraic generation of single domain computational grid for twin screw machines. Part II. Validation, *Advances in Engineering Software*, 109, 31-43. doi.org/10.1016/j.advengsoft.2017.03.001

Moosania, S. M. & Zheng, X. (2016). Comparison of Cooling Different Parts in a High Pressure Ratio Centrifugal Compressor. MDPI, Appl. Sci., 7, 16; doi:10.3390/app7010016

Patel, B., Kovacevic, A., Charogiannis, A., Alam, M. N., & Schütte, M. (2021). The use of laser-induced fluorescence to measure temperature in the leakage gaps of oil-free positive displacement rotary machines. Measurement: Journal of the International Measurement Confederation, 185(August), 110057. https://doi.org/10.1016/j.measurement.2021.110057

Patel, B., Kovacevic, A., Charogiannis, A., & Md nahinul Alam. (2021). Development of State-of-the-art Experimental Technique to Investigate Temperature Field in Leakage Flows of Positive Displacement Machines.

Rane, S., Stosic, N., & Dhunput, A. (2014). Prediction of Heat Transfer and Visualisation of Temperature Field in Screw Compressors. https://doi.org/10.1115/imece2014-37439

Rane, S. & Kovačević, A. (2017a). Application of numerical grid generation for improved CFD analysis of multiphase screw machines, 10th International conference on compressors and their systems, London, IOP Conf. Ser.: *Mater. Sci. Eng.*, 232, 01. DOI:10.1088/1757-899X/232/1/012017

Rane, S. & Kovačević, A. (2017b). Algebraic generation of single domain computational grid for twin screw machines. Part I. Implementation, *Advances in Engineering Software*, 107, 38-50. doi.org/10.1016/j.advengsoft.2017.02.003

Rane, S., Kovačević, A., Stošić, N. & Smith, I. (2021a). Analysis of real gas equation of state for CFD modelling of twin screw expanders with R245fa, R290, R1336mzz(Z) and R1233zd(E). *International Journal of Refrigeration*. 121:313-326. DOI: 10.1016/j.ijrefrig.2020.10.022.

Rane, S., Kovačević, A., Stošić, N. & Smith, I. (2021b). Bi-Directional System Coupling for Conjugate Heat Transfer and Variable Leakage Gap CFD Analysis of Twin-Screw Compressors. IOP Conf. Ser.: Mater. Sci. Eng. 1180 012001. doi.org/10.1088/1757-899X/1180/1/012001

Roclawski, H., Oberste-Brandenburg, C. & Böhle, M. (2018). Conjugate Heat Transfer Analysis of a Centrifugal Compressor for Turbocharger Applications. 16th ISROMAC 2016. Honolulu, hal-01884259.

Singh, G., Sun, S., Kovacevic, A., Li, Q. & Bruecker, C. (2019). Transient flow analysis in a Roots blower: Experimental and numerical investigations. Mechanical Systems and Signal Processing, 134, 106305. doi: 10.1016/j.ymssp.2019.106305

Speakman, J. (2019). Infrared thermography: Principles and applications. (September).

Stahl, M., Franz, h. Ittern, L. (2019). Conjugate Heat Transfer Study of a Centrifugal Compressor with Impeller Cavities. Global Power and Propulsion, Zurich. GPPS-TC-2019-0054.

Vittorini, D., Bianchi, G., & Cipollone, R. (2015). Energy saving potential in existing volumetric rotary compressors. Energy Procedia, 81, 1121–1130. https://doi.org/10.1016/j.egypro.2015.12.137

Zhang, Z., & Wu, W. (2021). Numerical investigation of thermal deformation of meshing pairs in single screw compressor. Applied Thermal Engineering, 188(January), 116614. https://doi.org/10.1016/j.applthermaleng.2021.116614

ACKNOWLEDGMENT

Funding for this research was received from Royal Academy of Engineering, UK, and Howden Compressors, UK, towards the project Smart Efficient Compression: Reliability & Energy Targets (SECRET), RAEng grant RCSRF2021\11\43.